Colin, M.E.G.D., T.F. Duda, L.A. te Raa, T. van Zon, P.J. Haley, Jr., P.F.J. Lermusiaux, W.G. Leslie, C. Mirabito, F.P.A. Lam, A.E. Newhall, Y.-T. Lin, J.F. Lynch, 2013. Time-Evolving Acoustic Propagation Modeling in a Complex Ocean Environment, OCEANS - Bergen, 2013 MTS/IEEE , vol., no., pp.1,9, 10-14 June 2013, doi: 10.1109/OCEANS-Bergen.2013.6608051

Time-Evolving Acoustic Propagation Modeling in a Complex Ocean Environment

M. E. G. D. Colin[1], T. F. Duda[2], L. A. te Raa[1], T. van Zon[1], P. J. Haley Jr.[3], P. F. J. Lermusiaux[3], W. G. Leslie[3], C. Mirabito[3], F. P. A. Lam[1], A. E. Newhall[2], Y.-T. Lin[2], J. F. Lynch[2]

[1] TNO, The Hague, The Netherlands
[2] Woods Hole Oceanographic Institution, Woods Hole, MA USA
[3] Massachusetts Institute of Technology, Cambridge, MA USA

***Abstract*— During naval operations, sonar performance estimates often need to be computed in-situ with limited environmental information. This calls for the use of fast acoustic propagation models. Many naval operations are carried out in challenging and dynamic environments. This makes acoustic propagation and sonar performance behavior particularly complex and variable, and complicates prediction. Using data from a field experiment, we have investigated the accuracy with which acoustic propagation loss (PL) can be predicted, using only limited modeling capabilities. Environmental input parameters came from various sources that may be available in a typical naval operation.**

The outer continental shelf shallow-water experimental area featured internal tides, packets of nonlinear internal waves, and a meandering water mass front. For a moored source/receiver pair separated by 19.6 km, the acoustic propagation loss for 800 Hz pulses was computed using the peak amplitude. The variations in sound speed translated into considerable PL variability of order 15 dB. Acoustic loss modeling was carried out using a data-driven regional ocean model as well as measured sound speed profile data for comparison. The acoustic model used a two-dimensional parabolic approximation (vertical and radial outward wavenumbers only). The variance of modeled propagation loss was less than that measured. The effect of the internal tides and sub-tidal features was reasonably well modeled; these made use of measured sound speed data. The effects of nonlinear waves were not well modeled, consistent with their known three-dimensional effects but also with the lack of measurements to initialize and constrain them.

Keywords—sonar performance prediction; acoustic modeling, ocean modeling, internal waves, shallow water acoustics

I. INTRODUCTION

Highly variable acoustic propagation conditions were observed in the field during the USA Office of Naval Research Shallow Water 2006 experiment (SW06) [1]. Here, results from a project to evaluate the ability of data-constrained acoustic propagation modeling to replicate the observations are reported. This type of modeling may be key to improving sonar performance predictions. The experiment was carried out on the New Jersey shelf, in an area with highly variable oceanographic conditions [2,3]. In particular, internal tides, nonlinear internal waves, eddies and the nearby shelf-break front impart strong variability on the sound speed field. All of these effects can be identified in the sound speed fields computed from temperature and salinity measurements. In addition, many smaller scale variations in sound speed are observed.

One component of the experiment was transmission from a moored source to horizontal/vertical line array receiver (HVLA). The path length was 19.6 km, extending from the northeast to the southwest, roughly aligned with the continental shelf break to the east. Temporally variable signals were recorded for this path, with ten days of signal analyzed here.

The signals were then modeled using two methods. A two-dimensional propagation model was run using 1) time-dependent measured profiles, and 2) time- and range-dependent profiles provided by the data-driven Multidisciplinary Simulation, Estimation and Assimilation System (MSEAS) ocean forecasting model [4]

Section II of this paper explains how this model testing fits into the context of sonar performance prediction modeling. Section III describes the measurements. Section IV describes the oceanographic and acoustic models and model results. Section V summarizes the findings.

II. SONAR PERFORMANCE MODELING

Performance modeling plays an important role in the use of sonar, as early as the design phase. The performance of all sonars depends heavily on the local properties of the water column, as well as that of its interfaces. Sonar performance models (SPM) are used for naval operations during the planning and execution phases. During the planning phase, models use environmental input from historical databases [5] or, when available, the information provided by an oceanographic model [4]. During the execution of an operation, a higher level of detail is required and these data are supplemented by in-situ measurements of the environment properties. These measurements provide a better accuracy than predictions or databases but are, in most cases, punctual samples, both temporally and spatially.

Sonar performance is generally represented by either active or passive sonar equations. The term “sonar equation” is broad and its level of complexity can range from a back of the envelope computation to days of computations with numeric models. Depending on the purpose and sensitivity of the author, these equations are either expressed in terms of energies or mean squared pressure and ratios thereof, usually

Part of this work was sponsored by the Netherlands Ministry of Defence and the U.S. Office of Naval Research. Details of grants are found in the acknowledgement section.

converted to a decibel form. For the purpose of this paper, we will consider a form the active and passive sonar equations that evaluate the Signal to Background Ratio (SBR) (or echo excess), which has a direct role in sonar detection performance.

The active sonar equation can be written as

$$SBR = (SL - PL_{Tx} - PL_{Rx} + TS) - (BGL - PG) \qquad (1)$$

A partial description of each term is given in Table I. We will not give a complete definition of each term and refer the reader to reference literature [6,7] for more details. In this paper, we will focus on the influence of the properties of the water column on active sonar performance. The water column has an effect on all the terms of the sonar equation, but quite often, it is only taken into account through the propagation loss terms. However, the performance (gain in signal to background ratio) of usual signal processing algorithms (beamforming and matched filtering) can also be influenced by the properties of the water column. For instance, the influence of internal waves on beamforming gain has recently been demonstrated [8]. Similarly, the matched filter gain can be degraded by the target response as well as interference between closely spaced echo arrivals, either due to multi-path propagation or target highlights [7,9]. The background level (due to noise [10] and reverberation [11]) is also influenced by the propagation conditions but will not be considered here.

In this work, the goal is to quantify the effect of the variation of properties in the water column on active sonar performance using signals recorded in the ocean, and assess whether the effects are predictable using all available environmental data from the site, or subsets of that data. These variations can impact PL as well as PG as follows:

- The PL_{Tx} term, corresponding to the sound propagation loss between the sonar source and the target can be directly measured.
- The PG term corresponding to the processing gain due to matched filter and beamforming gain. The variations of beamforming gain in this experiment were studied in [8] The variation of the matched filter gain remains a topic of on-going research.

TABLE I. TERMS OF THE SONAR EQUATIONS

Abbreviation	Signification
SBR	Signal to Background Ratio
SL	Source Level
PL	Propagation Loss (Tx, transmission, Rx, reception)
TS	Target Strength
BGL	Background Level
PG	Processing Gain (beamforming gain and matched filter gain)

Data from SW06 are used for this (active) sonar assessment. As a byproduct, because the prediction involves the modeled or interpolated ocean state, we also assess the capability of a generally available parabolic equation acoustic propagation model [12] and a state of the art oceanographic model [4] to model observed variations. SW06 is described in more detail in Section III. Briefly, pulses were transmitted between fixed sources and receivers for a few weeks. To capture the variations in PL and PG and to observe them in the same way they would affect an active sonar, we chose to extract the maximum of the matched filtered output of the received hydrophone signals for one path for ten days. This detection process imitates processing in many active sonars. By picking the maximum, we capture both the effects of shadowing and interference but also possible loss of temporal coherence of the signal. After subtracting the source level and maximum matched filter gain, this quantity was compared with the maximum of the channel impulse response simulated with the acoustic model. For simplicity, this quantity will be called Matched Filter Loss (MFL) in the rest of the paper as its definition does not match the usual definitions of propagation loss [6,7].

III. FIELD MEASUREMENTS

SW06 was a joint multi-institution, multi-national experiment off the coast of New Jersey sponsored by the Office of Naval Research. Multiple acoustic experiments were undertaken [1]. A major goal of a moored acoustic system effort undertaken by the Woods Hole Oceanographic Inst. (WHOI) was to study the time-dependence of sound propagation behavior along multiple fixed paths in an area there the seabed properties were fairly well known. The reason for knowing the seabed properties is that a hallmark of shallow-water acoustics is strong sound interaction with the seabed, and knowing the local geo-acoustic properties reduces

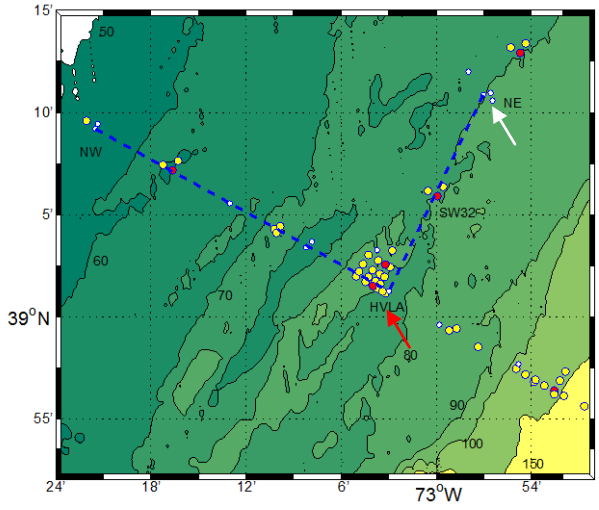

Fig. 1. Mooring locations for SW06 are shown. Pulses transmitted from station NE (White arrow) to the receiver HVLA (Red arrow) are analyzed here. Depth is contoured in meters. To the east is the shelf edge. Internal waves tend to propagate at heading near 300 degrees, so this propagation path is aligned with the majority of internal wave crests.

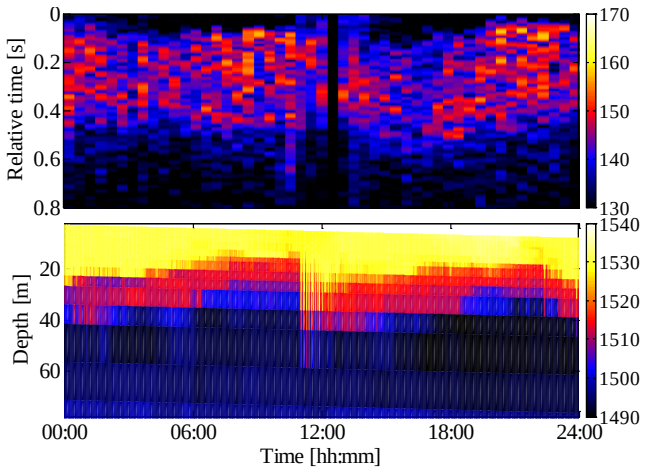

Fig. 2. (Top) Stacked matched filter responses in dB re μPa^2 for hydrophone 4 at a depth of 24.75 m. (Bottom) Corresponding measured sound speed profile at the receiver.

possible biases in the interpretation of the sound field characteristics. A complete description of the WHOI effort is available [13].

Only a subset of the effort is considered in this study. Broadband pulses were transmitted from station NE (Fig. 1) and received by the vertical portion of a combination horizontal/vertical line array (HVLA) hydrophone array 19.6 km away. This area featured strong variations in the water column properties, on a daily basis [15]. This setup allows monitoring the variations of some of the active sonar equation terms.

The unique combination of acoustic, moored environmental, shipboard, remote and AUV (Glider) measurements, along with the extensive characterization of the geo-acoustic parameters of the area [14,15] and data synthesis and analysis already carried out make this dataset an invaluable treasure of information for the study of sonar performance modeling.

A. *Environmental Measurements*

Many moorings (Fig. 1) recorded the passing of long-wavelength internal waves and short-wavelength nonlinear internal waves. The waves generally traveled to the northwest, as determined from the mooring records and ship-based observations, forming from the long-wavelength internal tides, evolving continuously, and constantly dissipating internal-wave energy [16,17]. The directionality of the waves was also measured from satellite images of surface-roughness internal-wave signatures [18]. The background environment through which the internal waves propagated featured the shelf/slope water front [19] which can heavily influence sound propagation by placing warm salty near the seabed, thereby refracting sound away from the seabed and causing sound-channel ducting.

For acoustic studies along the North East HVLA path (NE-HVLA), temperature, salinity, and pressure recordings from stacked moored sensors made once to twice per minute at HVLA, SW32, and NE (source position) were used. Sound-speed was computed from these using standard published equations [20]. The sound speed profiles were generally downward refracting.

B. *Acoustic Measurements*

A number of waveforms were transmitted during this experiment. We concentrated on a series of waveforms transmitted by the "Miami Sound Machine" (MSM) of the University of Miami and recorded by the WHOI HVLA "Shark" hydrophone array [13]. This array was deployed in an "L" configuration (horizontal and vertical) but only the vertical section (15 hydrophones) is considered here. The source and receiver were separated by 19.6 km on a somewhat bumpy seabed with a mean depth near 80 m.

The transmitted waveforms analyzed in this paper are trains of Maximum Length Sequences (MLS) [21] with an 813.8 Hz center frequency and a 200 Hz bandwidth. Each train consisted of a series of 75 511 digits-MLS. Each train lasted 90 s and was transmitted every 30 min.

The entire pulse train was matched-filtered (using a circular buffer, as required) and the squared matched-filtered outputs of all the sequences were then averaged. The resulting intensity time series were then divided by the MSM source level as well as the theoretical maximum matched filter gain (equal to the number of digits in an individual MLS), and converted to pressure using the known receiver sensitivity. Loss was then computed as follows,

$$\mathrm{MFL} = 10\log_{10}\left(\frac{\max\overline{\left|p(t)*r(t)\right|^2}}{NS_E}\right) \qquad (2)$$

where $p(t)$ is the measured pressure time series, $r(t)$ the transmitted replica, N the number of digits in the MLS and S_E the source energy factor. The horizontal bar above the matched filter output term denotes the pulse-train averaged. Fig. 2 shows 24 hours of MFL examples (48 pulse trains). As the quantity is different from the usual definition of PL, as it includes the variations in Matched Filter Gain as well as Propagation Loss, we refer to it as matched filter loss (MFL). This quantity includes the losses due to propagation as well as coherence.

IV. MODELING

The modeling required to test the accuracy of PL predictions in SW06 (hindcasts actually, but computed with information judged to be available for nowcasts or forecasts) consists of a few parts: generation of a volumetric field of sound speed in the study area, and sound propagation modeling under those conditions. Two PL predictions were done using sound-speed fields garnered in two ways, with progressing field complexity:

- Time- and range-dependent sound-speed profiles measured at the receiving array and at other stations on the path. The combination of this measurement based model and the acoustic propagation model will be referred to as "Model 1"

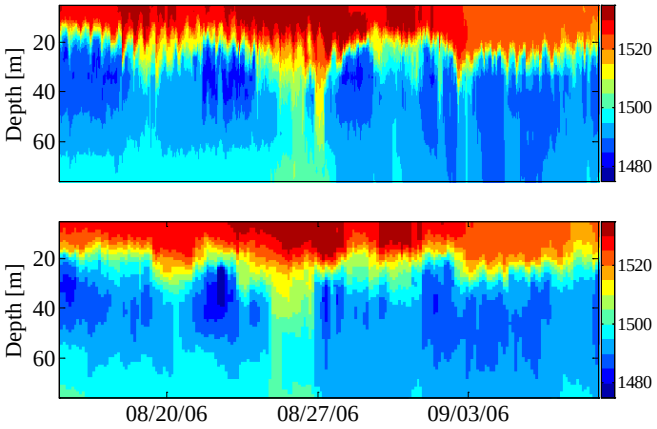

Fig. 3. Time series of measured (top) and modeled (bottom) sound speed profiles at HVLA are shown.

- Time- and range-dependent sound-speed profiles generated by the data-driven MSEAS model. These predictions were produced with a 3h sampling interval. This model in combination with the acoustic propagation model will be referred to as "model 2".

A. Measurement-based environmental model

The sound speed profiles measured at the HVLA, SW32, and NE moorings were used to build range-dependent sound-speed profiles in the NE-HVLA slice using interpolation A time step of 20 min was used to update conditions.

B. Data-driven dynamical oceanographic model

The Multidisciplinary Simulation, Estimation, and Assimilation System ([4,21]) is used to study and quantify tidal- to mesoscale processes and physical-biogeochemical interactions over multi-resolution domains. For physics, MSEAS contains both hydrostatic and non-hydrostatic codes; for biology, a generalized adaptable biogeochemical modeling system [23], with varied options for biological parameterizations and components. Capabilities include implicit two-way nesting [4]. A high-order finite element code on unstructured grids is built for non-hydrostatic physics and biogeochemical dynamics at shelf breaks [24]. Other MSEAS subsystems include: initialization schemes, nested data-assimilative tidal prediction; fast-marching coastal objective analysis ; stochastic sub-grid-scale models; data assimilation, optimization and adaptive sampling; dynamically-orthogonal-equation for uncertainty predictions; non-Gaussian assimilation using Gaussian Mixture Models; machine learning of model structures and functions; and Lagrangian Coherent Structures. MSEAS has been used for multiple focused scientific studies in shelfbreak regions [4, 23, 25-30].

The MSEAS model was run in real-time forecast mode during SW06. The results illustrated in this paper are not from the real-time simulations, but rather from a subsequent re-analysis. Satellite and ship-obtained data (e.g. CTD, XBT, Scanfish) have been assimilated. Mooring data are not assimilated, thus providing an independent evaluation data set. The reanalysis is a free surface simulation employing two-way implicit nesting with tidal and atmospheric forcing. The modeling domain includes 100 terrain-following vertical levels with a horizontal resolution of 1 km. The configuration of MSEAS for this particular application allows for the prediction of internal tides (long internal waves near tidal frequencies, directly forced by tides), but does not allow for the prediction of high-frequency internal-wave packets.

A time series of observed sound speed at a mooring is compared to that simulated by MSEAS in Fig. 3. There is very good qualitative and quantitative agreement between the data and model. The long- term variations in thermocline depth, reflected in the thickness of the upper layer of high sound speed, are captured by the model. In particular, the deeper upper layer between August 25 and August 27 is evident in the measurements and well-represented the model results. The effect of the passage of Tropical Storm Ernesto can be seen in the MSEAS sound speed after September 3, with an extended period of a deeper mixed layer, and reduced sound speeds in the mixed layer. Instances of sound speed minima around 35 m -40 m seen in the data throughout are apparent in the MSEAS simulations. These minima are well correlated in temporal structure, physical structure, and value.

Many improvements to the re-analysis utilized here were completed and are expected to further improve subsequent applications. They include: levels optimized to the thermocline structure; the use of corrected evaporation-precipitation and direct fluxes from the Weather Research and Forecast Modeling System and the Navy Operational Global Atmospheric Prediction System for atmospheric forcing; the correction of amplitudes in the diurnal tidal components; higher resolution tidal forcing; implementation of a sponge to reduce tidal reflections at open boundaries; and, upgraded initial conditions incorporating synoptic data and pseudo profiles to bolster the front, World Ocean Atlas [5] climatology corrected to match 2006 slope conditions, a revised shelfbreak temperature-salinity front feature model, a Gulf Stream temperature-salinity feature model (based on synoptic data) and transport feature models for each of the Gulf Stream, slope recirculation gyre and shelfbreak front. The data assimilation methodology was tuned for the front and tides through the use of shorter space scales and weaker, more frequent assimilation. Model sub-grid scale parameters (vertical mixing, horizontal mixing and bottom friction) were also re-tuned.

The MSEAS approach to acoustic modeling is based on coupling realistic data-assimilative environmental and acoustic propagation models with distributed, parallel ensemble simulations. Initial efforts that have coupled four-dimensional ocean fields with 2D acoustics modeling include data assimilation and uncertainty studies [31,32], end-to-end computations [33], real-time at-sea predictions [25] and coupled adaptive sampling [34].

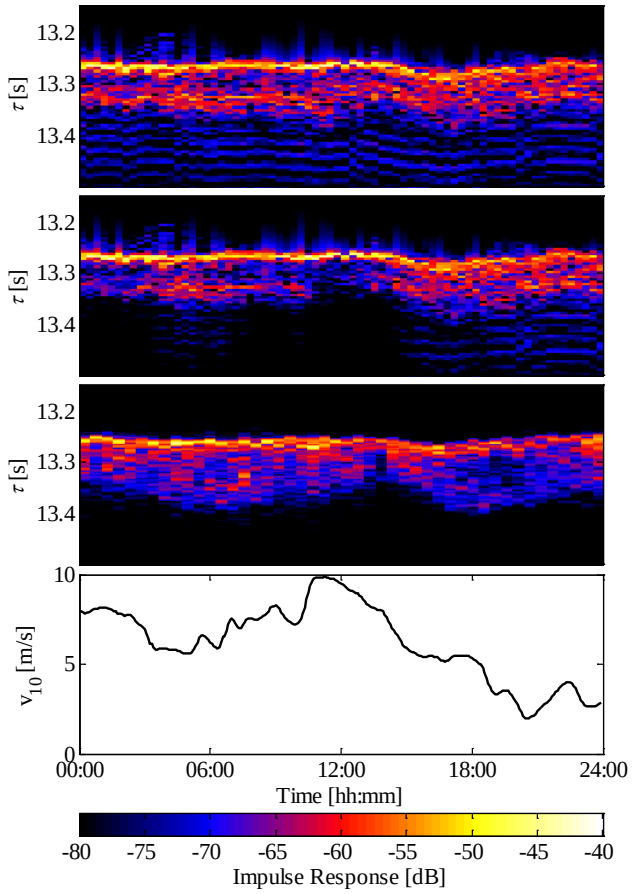

Fig. 4 (top) 800-Hz impulse responses for the 08.21.06 at 36 m depth simulated for one day using a perfectly reflecting surface and measured date and range-dependent conditions (Model 1). (middle) Impulse responses simulated in the same manner except a rough surface and bubble layer are added. (third plot from the top) Measured impulse response for the same time period. (bottom) Measured local wind speed at 10 m altitude.

C. *Acoustic model*

Within vertical slices obtained from the sound-speed modeling, the code RAM [12] was used for acoustic field calculations. The impulse response of the channel in the frequency band of the transmission was computed by means of Fourier synthesis: pure tone pressure fields, (i.e. spectral levels of pressure) were computed with RAM for an array of frequencies within the band of interest; and an inverse Fourier transform was then applied to these pressure fields to obtain the channel impulse response

$$h(\tau_n) = \frac{\sqrt{B}}{N} \sum_{k=1}^{N} P(f_k)\, e^{2\pi j \frac{(n-1)(k-1)}{N}}, \qquad (3)$$

where B is the signal bandwidth (200 Hz), $P(f_k)$ the pressure field at frequency f_k, τ_n is the delay and N the number of Fourier coefficients.

TABLE II. SUMMARY OF GEO-ACOUSTIC PARAMETERS

Layer	Thickness	Sound speed	Attenuation
Sediment	10 m	1670 m/s	0.15 dB/λ
Substrate	-	1725 m/s	0.15 dB/λ

The PL levels are sensitive to seafloor properties in downward-refracting environments such as that of SW06 (see Fig. 3). A geo-acoustic model kindly provided by Dr. Ballard [14], as well as results from [15], were used to parameterize the seafloor.

When comparing the resulting impulse response with measured impulse response, it appeared that the initially-used perfectly reflecting sea surface assumption was insufficient to represent the impulse response. Indeed, the resulting impulse response features very high "later" arrivals. A version of RAM allowing the use of a rough surface was modified to also include the possibility of inputting a depth variable attenuation profile. Following the approach described in [35], we augmented the sound speed profiles used for the computations with a representation of layer of bubbles, by altering the sound speed and attenuation of the surface layer. The rough surface

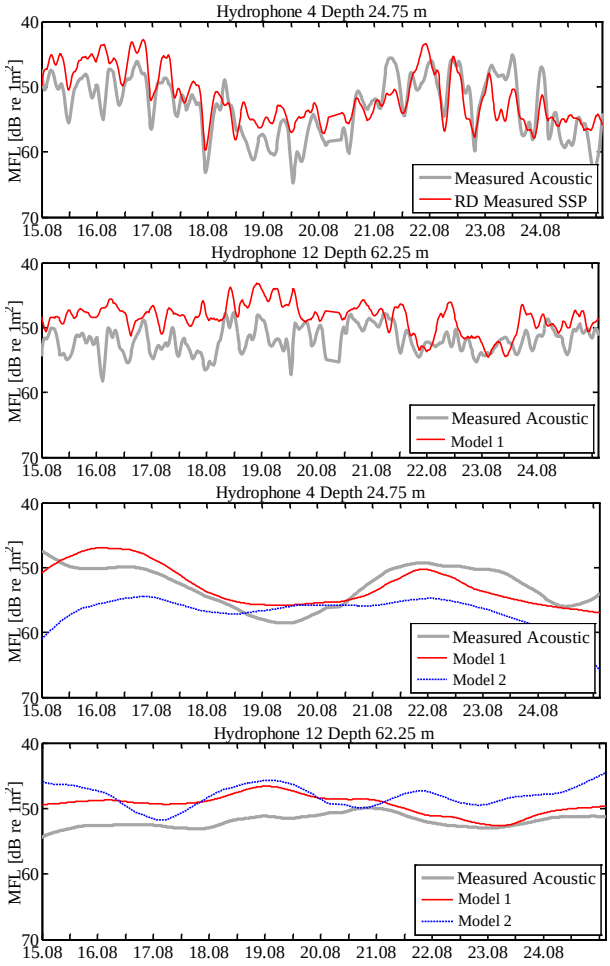

Fig. 5 (top) Measured and modeled (Model 1) matched filter loss, filtered with a 2 h window at two depths. (bottom) measured and modeled (Model 1 and 2) propagation loss, filtered with a 24 h window at the same depths

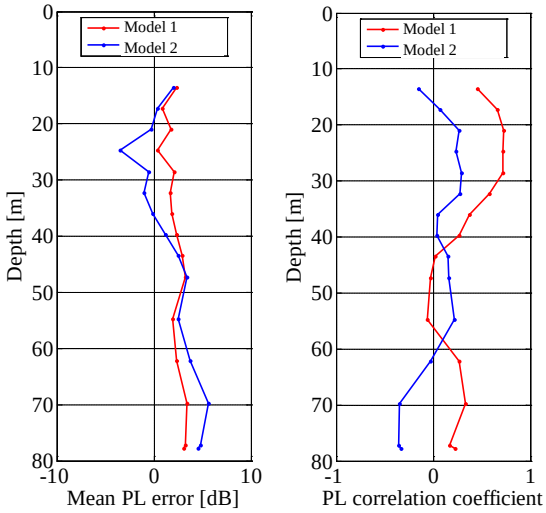

Fig 6. (left) Average PL error of the PL modeled with Model 1 (Red) and Model 2 (Blue). The error sequence was computed using a 2 h low pass filter. (right) Correlation coefficient of the modeled propagation loss sequences with the measured propagation loss.

was then represented by a realization of the Pierson-Moskowitz spectrum corresponding to the measured wind speed [36]. The results are shown in Fig. 4, compared to measured data. The effect of the addition of the wind effect is directly visible on the shape of the impulse responses. The reduction of the later arrivals intensity is especially visible in the first half of the day. This modeling of the effect of wind was developed too late to be integrated in the complete modeling analysis, but will be used in later studies.

D. Model results

The acoustic modeling was done for ten days yielding enough degrees of freedom to compute statistics. The simulated MFL was computed using the peak level of the simulated broadband impulse response. First of all, the resulting propagation losses are compared to the measured propagation losses at two receiver depths in Fig. 5.

Both acoustic and oceanographic models are limited by practicality to contain only a subset of the true ocean feature dynamic range and ocean physics. An important problem is that sets of small-scale internal waves in the ocean have first-order effects on intensity, but are not included in either the interpolated-data model (model 1, range dependent measured sound speed profiles (SSP)) or the MSEAS dynamical model (model 2). As a result, the measured acoustic MFL is more variable. However, model 1 *does* contain the internal tide, and *does* produce temporal behavior that mimics reality (see the top of Fig. 5). This is because the packets are often synchronized with the internal tide, and the model is producing internal tide-induced acoustic fluctuations, while the ocean has (partially) synchronized internal tide-induced and small-scale internal wave-induced fluctuations.

Perhaps a more sensible evaluation of both models is to low-pass filter the observed MFL fluctuations, to attenuate the tidal-band synchronized short (high-frequency) waves and other higher frequency features that the models are not

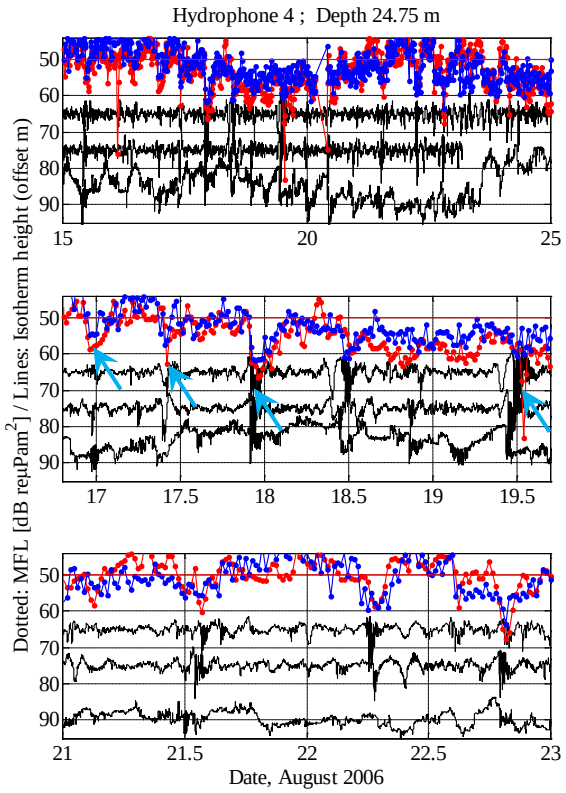

Fig 7. Simulated (Model 1) (blue dots) and measured (red dots) PL at 24.75 m depth superimposed with the estimated isopycnals height offset at the HVLA, at mooring (SW32) and at the MSM. The blue arrows denote internal waves event during which the mismatch between modeled and measured PL was most noticeable.

intended to reproduce. The lower part of Fig. 5 shows the comparison. Neither the measurement-only modeling (Model 1) nor the data-driven modeling (Model 2) reproduce the mean MFL and the MFL fluctuations. We believe that this is caused by three-dimensional acoustic propagation processes that are not included in the acoustic modeling module of the SPM tested here. Other reasons for these differences could also be found in the quality of the input parameters, such as seabed model or sound speed profile. For instance, three measurements of the sound speed profile interpolated along the acoustic paths might be insufficient to represent internal waves. This is especially visible in Fig. 7 in which unfiltered modeled (using measured SSP, Model 1) and measured MFL are shown superimposed with estimated displacements of mid-water column isopycnals. These were computed from either vertically-averaged then time integrated ADCP vertical velocities, or vertically interpolated temperature time-series obtained at a collection of fixed depths, at three locations along the acoustic path. Underestimations of MFL (blue arrows) of the model can be matched to internal wave events, visible in the superimposed isopycnals.

Despite the lack of strong correlation between the modeled and observed MFL time series, the mean (over time) differences between model MFL and measured MFL are shown in Fig 6. The agreement is best near the surface (15 m to

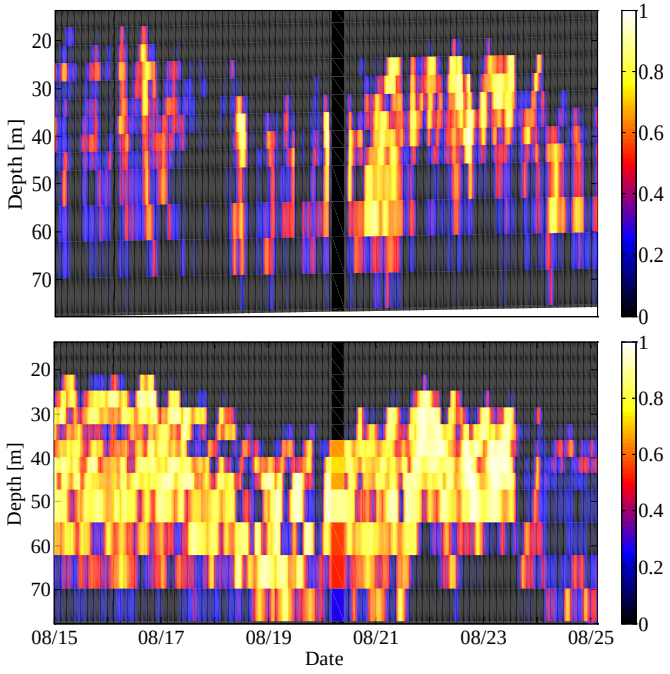

Fig. 8 Probability of detection for a fictive sonar computed using measured (top) and data-driven modeled (bottom) propagation loss as a function of time and target depth.

30 m depth). At depths greater than 50 m the measured MFL is greater than the modeled, seen in Fig 5. The models have different error behavior over depth; model 1 has an error that is a weak function of depth, while model 2 has an error trend.

To illustrate the influence of the mismatch in estimated MFL on estimated sonar detection performance, we constructed a simple noise limited active sonar performance scenario. The MFL simulated using the measured profiles (Model 1), as well as the measured MFL were used. All the other terms were kept constant. The receiver was chosen as a single hydrophone, resulting in a null beamforming gain. The source and receiver depth correspond to the MSM source depth (60 m). The potential targets are situated at the depth of the HVLA hydrophones. The other parameters are summarized in Table III. These values do not represent a specific sonar, realistic target or background level but were chosen to obtain observable variations in probability of detection using both measured and simulated MFLs. Had the parameters been chosen such that either a very high or low SBR would have been obtained, the probability of detection would either be one or zero and therefore not illustrative. The differences in probability of detection shown here can be interpreted as an upper bound.

TABLE III. TERMS OF THE SONAR EQUATIONS

Abbreviation	Value
SL	200 dB re μ Pam^2
PL	$2PL_{Tx}$ (Measured or Simulated)
TS	0 dB re m^2
BGL	90 dB re μ Pa^2
PG	Beamforming Gain 0 dB (Matched filter Gain contained in PL term)

The detection process represented here is a constant false alarm rate detector, in which a desired probability of false alarm is chosen and the resulting probability of detection can then be estimated. For simplicity, we assumed a Rayleigh distribution for the target echo and Gaussian distribution for the background. We then computed the probability of detection p_d for a typical probability of false alarm (p_{fa}) of 10^{-6} [6] using the following formula [7]:

$$p_d = p_{fa}^{1/(1+\rho)}, \quad (4)$$

in which ρ is the signal to background ratio. The probability of detection computed using the measurements is interpreted as the actual probability of detection for this situation.

The results are shown in Fig. 8. The effect of the global variations of the thermocline height can be seen in both pictures, but the probability of detection is clearly overestimated by Model 1. This model, if used in an operational situation, would predict steady reliable detections under the thermocline (p_d around 0.8), while the sonar operator would observe highly variable detection performance (p_d under 0.5).

V. DISCUSSION AND CONCLUSION

We have modeled broadband propagation effects using a data-driven and model-driven 2D acoustic propagation model. The acoustic model input were computed with a state of the art oceanographic model used in near operational forecast conditions. The acoustic model outputs were compared with measurements. The data-driven acoustic predictions could reproduce some of the low frequencies measured variations (internal tide, long term depth variation of the thermocline) while others could not be captured (internal wave). This was attributed to the fact that the acoustic model does not include 3D processes such as horizontal refraction due to non-linear internal waves that are known to occur in this area. Seabed properties can also be a factor. The data-driven acoustic predictions were used to generate estimates of probability of detection, using the acoustic measurements to generate reference values. The probability of detection values was very sensitive to the error in propagation loss prediction.

When confronted with frequent mismatch between performance predictions and their own observations, operators very quickly lose confidence in a modeling system. The

obvious course of action is to improve the quality of the modeling and of the inputs that it requires. The shortcomings of the acoustic model shown here are addressed, for instance through the development of 3D acoustic propagation models [38]. Another necessary measure is to accompany predictions with a measure of uncertainty. This has been done in the context of passive sonar, for the influence of the water column on propagation loss [27,32,39,40] and beamforming gain [8] and the influence of uncertainty in bottom reflection properties on propagation prediction [41]. The complexity is increased for active sonar performance prediction. The active sonar equation contains a few more terms than the passive sonar equation, such as reverberation level (contained in the background level) or matched filter gain (contained in the processing gain). Back scattering parameters are usually estimated through inversions, the resulting accuracy depending then on the quality of the method and subsequent model [42,43]. The variability of matched filter gain in shallow water will be the topic of future studies.

More advanced re-analyses of the SW06 experiment have been carried out since this study was completed. More specifically, the MSEAS model has been run again with higher resolution and with improved initial conditions and boundary conditions, yielding ocean fields that are designed to more closely resemble reality. Future activities will include using these fields to recompute the statistics presented here.

ACKNOWLEDGMENT

The authors thank the SW06 partners. The TNO work was sponsored by the Defense Materiel Organization of the Dutch MoD. The TNO authors thank Dr. Ballard for providing her geo-acoustic model and Dr. Ainslie and Lt Cdr De Jong for their useful comments. The WHOI PI's acknowledge the support of the Office of Naval Research Ocean Acoustics Program. The MSEAS group (PFJL, PJH, WGL and CM) is very grateful to the Office of Naval Research for support under grants N00014-12-1-0944 (ONR6.2), N00014-08-1-1097 (ONR6.1) and N00014-08-1-0680 (PLUS-SEAS) to the Massachusetts Institute of Technology (MIT). The MSEAS group thanks G. Gawarkiewicz, P. Abbot and T. Duda for their ocean data and M. Taylor and J. Hare for their NMFS survey data. They also thank J. Evans, S. Glenn, and J. Wilkin for their real-time WRF atmospheric fluxes and J. Doyle, D. Marble, J. Nachimkin and J. Cook for the FNMOC atmospheric products. The MSEAS group also acknowledges the OTIS tidal products, created at Oregon State University by G. Egbert and L. Erofeeva.

REFERENCES

[1] D. Tang, J. N. Moum, J. F. Lynch, P. A. Abbot, R. Chapman, P. H. Dahl, T. Duda, G. Gawarkiewicz, S. Glenn, J. A. Goff, H. Graber, J. Kemp, A. Maffei, J. Nash and A. Newhall, "Shallow Water 2006: A joint acoustic propagation/nonlinear internal wave physics experiment," Oceano-graphy, vol. 20(4), pp. 156-167, 2007

[2] C. A. Linder and G. Gawarkiewicz, "A climatology of the shelfbreak front in the Middle Atlantic Bight," J. Geophys. Res., vol. 103(C9), pp. 18,405-18,423, 1998.

[3] J. R. Apel, M. Badiey, C.-S. Chiu, S. Finette, R. Headrick, J. Kemp, J. F. Lynch, A. Newhall, M. H. Orr, B. H. Pasewark, D. Tielbuerger, A. Turgut, K. von der Heydt and S. Wolf.. "An overview of the 1995 SWARM shallow water internal wave acoustic scattering experiment," IEEE J. Oceanic Eng., vol. 22, pp. 465–500, 1997.

[4] P. J. Haley Jr., P.F. Lermusiaux, "Multiscale two-way embedding schemes for free-surface primitive equations in the 'Multidisciplinary Simulation, Estimation and Assimilation System'," Ocean Dyn., vol. 60(6), pp. 1497-1537, 2010.

[5] R. A. Locarnini, A. V. Mishonov, J. I. Antonov, T. P. Boyer, and H. E. Garcia, "World Ocean Atlas 2005, Volume 1: Temperature," in NOAA Atlas NESDIS 61, S. Levitus, Ed. Washington, D.C.: U.S. Government Printing Office, 2006.

[6] R.J. Urick, Principles of Underwater Sound, NewYork: McGraw-Hill. 1975.

[7] M. A. Ainslie, Principles of Sonar Performance Modeling, Chichester, U. K.: Praxis/Springer, 2010

[8] T. F. Duda, J. M. Collis, Y. T. Lin, A. E. Newhall, J. F. Lynch, and H. A. DeFerrari, "Horizontal coherence of low-frequency fixed-path sound in a continental shelf region with internal-wave activity," J. Acoust. Soc. Am., vol. 131, pp. 1782-1797, 2012.

[9] J. P. Hermand, & W. I. Roderick, "Acoustic model-based matched filter processing for fading time-dispersive ocean channels: Theory and experiment.," IEEE J. Oceanic Eng., vol. 18(4), pp. 447-465, 1993.

[10] W. A. Kuperman and F. Ingenito, "Spatial correlation of surface generated noise in a stratified ocean.," J. Acoust. Soc. Am., vol. 67, pp 1988-1996, 1980.

[11] D. D. Ellis, "A shallow-water normal-mode reverberation model.," J. Acoust. Soc. Am., vol. 97, pp. 2804-2814, 1995.

[12] M. D. Collins, "A split-step Padé solution for the parabolic equation method," J. Acoust. Soc. Am., vol. 93, 1736-1742, 1993.

[13] A. E. Newhall, T. F. Duda, K. von der Heydt, J. D. Irish, J. N. Kemp. S. A. Lerner, S. P. Liberatore, Y.-T. Lin, J. F. Lynch, A. R. Maffei, A. K. Morozov, A. Shmelev, C. J. Sellers, and W. E. Witzell, "Acoustic and oceanographic observations and configuration information for the WHOI moorings from the SW06 experiment," Woods Hole Oceanographic Institution Technical Report No. WHOI-2007-04, 2007.

[14] M. S. Ballard, K. M. Becker, J.A. Goff, . "Geoacoustic inversion for the New Jersey shelf: 3-D sediment model," IEEE J. Oceanic Eng., vol. 35(1), pp. 28-42, 2010.

[15] S. D. Rajan, K. M. Becker. "Inversion for range-dependent sediment compressional-wave-speed profiles from modal dispersion data," IEEE J. Oceanic Eng., vol. 35(1), pp. 43-58, 2010.

[16] E. L. Shroyer, J. N. Moum and J. D. Nash, "Energy transformations and dissipation of nonlinear internal waves over New Jersey's continental shelf," Nonlin. Processes Geophys., vol. 17, pp. 345–360, 2010.

[17] E. L. Shroyer, J. Moum and J. Nash, "Nonlinear internal waves over New Jersey's continental shelf," J. Geophys. Res., vol. 116, 2011

[18] J. F. Lynch, Y.-T. Lin, T. F. Duda and A. E. Newhall, "Acoustic ducting, reflection, refraction, and dispersion by curved nonlinear internal waves in shallow water," IEEE J. Oceanic Eng., vol. 35, pp. 12-27, 2010.

[19] J. F. Lynch, C. Emerson, P. A. Abbot, G. G. Gawarkiewicz, A. E. Newhall, Y.-T. Lin, and T. F. Duda, "On whether azimuthal isotropy and alongshelf translational invariance are present in low-frequency acoustic propagation along the New Jersey shelfbreak," J. Acoust. Soc. Am., vol. 131, pp. 1762-1781, 2012.

[20] K. V. Mackenzie, "Nine-term equation for sound speed in the oceans." J. Acoust. Soc. Am., vol. 70, pp. 807-812, 1981

[21] W. Munk, P. Worcester and C. Wunsch, Ocean Acoustic Tomography, New York: Cambridge U. Press, 1995.

[22] W. G. Leslie, P. J. Haley Jr., P. F. J. Lermusiaux, M. P. Ueckermann, O. Logutov and J. Xu, 2010. "MSEAS Manual,".MSEAS Report-06, 2010.

[23] P. F. J. Lermusiaux, "Adaptive Modeling, Adaptive Data Assimilation and Adaptive Sampling." Special issue on "Mathematical Issues and Challenges in Data Assimilation for Geophysical Systems: Interdisciplinary Perspectives," C.K.R.T. Jones and K. Ide, Eds. Physica D, vol 230, pp. 172-196. 2007.

[24] M. P. Ueckermann and P. F. J. Lermusiaux. "High Order Schemes for 2D Unsteady Biogeochemical Ocean Models," Ocean Dyn., vol. 60, pp. 1415-1445, 2010

[25] F. P. A. Lam, P. J. Haley Jr., J. Janmaat, P. F. J. Lermusiaux, W. G. Leslie, and M. W. Schouten. “At-sea Real-time Coupled Four-dimensional Oceanographic and Acoustic Forecasts during Battlespace Preparation 2007,” J. Mar. Sys., vol. 78, Supplement, Special issue on "Coastal processes: challenges for monitoring and prediction," 2009.

[26] P. J. Haley Jr., P. F. J. Lermusiaux, A. R. Robinson, W. G. Leslie, O. Logutov, G. Cossarini, X. S. Liang, P. Moreno, S. R. Ramp, J. D. Doyle, J. Bellingham, F. Chavez, and S. Johnston, “Forecasting and Reanalysis in the Monterey Bay/California Current Region for the Autonomous Ocean Sampling Network-II Experiment,” Deep-Sea Res. II, vol. 56, pp. 127-148, 2009

[27] P. F. J. Lermusiaux, , J. Xu, C. F. Chen, S. Jan, L. Y. Chiu and Y. -J. Yang. “Coupled Ocean-Acoustic prediction of transmission loss in a continental shelfbreak region: predictive skill, uncertainty quantification and dynamical sensitivities,” IEEE J. Oceanic Eng., vol. 35(4), pp. 895-916. 2010.

[28] P. F. J. Lermusiaux, P. J. Haley, Jr., W. G. Leslie, A. Agarwal, O. Logutov and L. J. Burton, “Multiscale Physical and Biological Dynamics in the Philippines Archipelago: Predictions and Processes,” Oceanography, vol. 24(1), pp. 70-89, 2011.

[29] G. Gawarkiewicz, S. Jan, P. F. J. Lermusiaux, J. L. McClean, L. Centurioni, K. Taylor, B. Cornuelle, T. F. Duda, J. Wang, Y. J. Yang, T. Sanford, R.-C. Lien, C. Lee, M.-A. Lee, W. G. Leslie, P. J. Haley Jr., P. P. Niiler, G. Gopalakrishnan, P. Velez-Belchi, D.-K. Lee, and Y. Y. Kim. “Circulation and intrusions northeast of Taiwan: Chasing and predicting uncertainty in the cold dome,” Oceanography, vol. 24(4), pp. 110-121, 2011.

[30] S. R. Ramp, P. F. J. Lermusiaux, I. Shulman, Y. Chao, R. E. Wolf, and F. L. Bahr, “Oceanographic and Atmospheric Conditions on the Continental Shelf North of the Monterey Bay during August 2006,” Dyn. Atmos. Oceans, vol. 52, pp. 192-223, 2011.

[31] P. F. J. Lermusiaux and C.-S. Chiu. “Four-dimensional data assimilation for coupled physical-acoustical fields,” In Impact of Littoral Environmental Variability on Acoustic Predictions and Sonar Performance, N. G. Pace and F. B. Jensen, Eds., Dordrecht: Kluwer, pp. 417-424, 2002.

[32] P. F. J. Lermusiaux, C.-S. Chiu and A. R. Robinson. “Modeling uncertainties in the prediction of the acoustic wavefield in a shelfbreak environment,” In Theoretical and Computational Acoustics 2001: Beijing, China, 21-25 May 2001, E.-C. Shang, Q. Li and T.F. Gao, Eds., River Edge, NJ: World Scientific, pp 191-200, 2002.

[33] A. R. Robinson, and P. F. J. Lermusiaux. “Prediction systems with data assimilation for coupled ocean science and ocean acoustics.” In Theoretical and Computational Acoustics 2003: Honolulu, Hawaii, 11-15 August 2003, A. Tolstoy, Y.-C, Teng, and E-.C. Shang, Eds., River Edge, NJ: World Scientific, pp. 325-342, 2004.

[34] J. Xu, P. F. J. Lermusiaux, P. J. Haley Jr., W. G. Leslie and O. G. Logutov. “Spatial and Temporal Variations in Acoustic propagation during the PLUSNet-07 Exercise in Dabob Bay,” Proc. Meet Acoust., vol. 4, pp. 07001, 2008.

[35] R. van Vossen and M. A. Ainslie, “The effect of wind-generated bubbles on sea-surface backscattering at 940 Hz,” J. Acoust. Soc. Am., vol. 130(5), pp. 3413-3420, 2011.

[36] W. J. Pierson and L. Moskowitz, “A proposed spectral form for fully developed wind seas based on the similarity theory of SA Kitaigorodskii,” J. Geophys. Res., vol. 69.24, pp. 5181-5190, 1964.

[37] Y. T. Lin, A. E. Newhall, T. F. Duda, P. F. Lermusiaux, P. J. Haley Jr., . “Merging multiple-partial-depth data time series using objective empirical orthogonal function fitting,” IEEE J. Oceanic Eng., vol. 35(4), pp. 710-721, 2010.

[38] Y. T. Lin, J. M. Collis, T. F. Duda, “A three-dimensional parabolic equation model of sound propagation using higher-order operator splitting and Padé approximants,” J. Acoust. Soc. Am., vol. 132(5), pp. 364-370, 2012.

[39] P. Abbot and I. Dyer, “Sonar performance predictions incorporating environmental variability,” In Impact of Littoral Environmental Variability on Acoustic Predictions and Sonar Performance, F. B. Pace ans F. B. Jensen, Eds. Dordrecht: Kluwer, pp. 611-618, 2002.

[40] A. R. Robinson, P. Abbot, P. F. J. Lermusiaux, and L. Dillman, “Transfer of uncertainties through physical-acoustical-sonar end-to-end systems: a conceptual basis,” In Impact of Littoral Environmental Variability on Acoustic Predictions and Sonar Performance, N. G. Pace ans F. B. Jensen, Eds. Dordrecht: Kluwer, pp. 603-610, 2002.

[41] L. Sha and L. W. Nolte, “Effects of environmental uncertainties on sonar detection performance prediction,” J. Acoust. Soc. Am., vol. 117, pp. 1942-1953, 2005.

[42] C. W. Holland, “Fitting data, but poor predictions: Reverberation prediction uncertainty when seabed parameters are derived from reverberation measurements,” J. Acoust. Soc. Am., vol. 123, pp. 2553-2562, 2008.

[43] L. Abrahamsson, B. L. Andersson, S. Ivansson, J. Pihl, M.A. Ainslie, F. P. A. Benders, M. E. G. D. Colin, R. van Vossen, B. Chalindar, X. Cristol, B. Juhel, J. Dybedal, G. K. Olsen, E Eidem. “Stabilizing reverberation inversion by regression relations involving a grain size parameter.” J. Acoust. Soc. Am., vol. 130(4), pp. 2391-2391, 2011.